

PRESSURE- AND TEMPERATURE-CONTROLLED TIME-RESOLVED EMISSION SPECTROSCOPY  
APPLIED TO COORDINATION COMPOUNDS

H.-B. KIM, T. HIRAGA,<sup>1</sup> T. UCHIDA, N. KITAMURA,<sup>2</sup> and S. TAZUKE<sup>†</sup>

Research Laboratory of Resources Utilization, Tokyo Institute of Technology,  
4259 Nagatsuta, Midori-ku, Yokohama, 227 Japan.

<sup>†</sup>Deceased on July 11, 1989.

SUMMARY

Pressure effects on emission spectra of  $[\text{Pt}_2(\text{P}_2\text{O}_5\text{H}_2)_4]^{4-}$  ( $\text{Pt}_2^{4-}$ ) crystals and  $\text{Ru}(\text{bpy})_3^{2+}$  solution ( $\text{RuB}_3^{2+}$ , in ethanol-methanol) were studied. In  $\text{Pt}_2^{4-}$  crystals, reduction of both intra- and intermolecular Pt-Pt distances under high pressure resulted in lower energy shifts of fluorescence and phosphorescence, emergence of excimer-like emission, as well as in efficient T-T annihilation. In  $\text{RuB}_3^{2+}$  solution, pressure induced high energy shift and sharpening of the emission were observed at 110 - 200 K, and were interpreted by viscosity dependent solvent relaxation.

INTRODUCTION

Pressure effects on excited molecules are of current interest since the intramolecular factors (interatomic distance and bond angle, overlaps of atomic orbitals, and so forth) and intermolecular factors (morphology, crystals structure, intermolecular distance and orientation, free volume of medium, and so forth) can be tuned by variation of the applied pressure without changing the chemical composition. These structural changes influence both absorption and emission spectra of organic/inorganic molecules so that inter- and/or intramolecular interactions in the ground and excited states could be elucidated by "pressure tuning spectroscopy" (ref. 3). In solid, intra- and intermolecular distances are compressed under high pressure. Therefore, exciton migration, electron hopping, spin-orbit coupling, and so forth, sensitive to the distance between adjacent molecules or atoms, will be under the influence of pressure. In solution, on the other hand, the primary effect of pressure is the change in solvent properties; viscosity ( $\eta$ ), dielectric constant ( $D_s$ ), and refractive index ( $n$ ). Solvation around polar excited state molecules will be thus susceptible to pressure. Although temperature variation can also change these solvent parameters, the effects of temperature and solvent parameters can not be discussed independently.

Pressure- and temperature-controlled experiments provide complementary information on the photophysical processes in solution.

In this article, we present the pressure effect on the emission spectra of well-grown  $[\text{Pt}_2(\text{P}_2\text{O}_5\text{H}_2)_4]^{4-}$  ( $\text{Pt}_2^{4-}$ ) crystals (ref. 4) and  $\text{Ru}(\text{bpy})_3^{2+}$  ( $\text{RuB}_3^{2+}$ ) solution (ref. 5). Characteristics of  $\text{Pt}_2^{4-}$  and  $\text{RuB}_3^{2+}$  are as follows.

$\text{Pt}_2^{4-}$  consists of two square planar complexes facing each other in which a Pt atom is located on the center of each plane (refs. 6-7). Furthermore, in the well-grown crystals the  $\text{Pt}_2^{4-}$  unit aligns along the Pt-Pt axis. The intramolecular Pt-Pt distance and the intermolecular  $\text{Pt}_2^{4-}$  distance along the Pt-Pt axis in the crystals (as potassium salt) are 2.925 and 5.063 Å, respectively. The Pt-Pt interaction is weak and expected to be affected by applied pressure, leading to the change in  $d_{z^2}$  orbital energy of mutually facing metal ions. Since  $\text{Pt}_2^{4-}$  exhibits both strong phosphorescence with long lifetime ( $\mu\text{s}$ ) and fluorescence with much short lifetime (ps), pressure-induced structural changes of the crystals will be easily monitored by emission spectroscopy.

The metal-to-ligand charge-transfer (MLCT) excited state of  $\text{RuB}_3^{2+}$ , represented as  $^*[ \text{Ru}^{\text{III}}(\text{bpy})_2(\text{bpy}^-) ]^{2+}$ , possesses a large dipole moment while the complex is non-polar in the ground state (ref. 8). Excitation of  $\text{RuB}_3^{2+}$  thus accompanies large reorientation of the surrounding solvent molecules. Pressure- and temperature-controlled time resolved emission spectroscopy are potential means to study solvent relaxation of  $^*\text{RuB}_3^{2+}$ .

## INSTRUMENTAL SETUP

### High-pressure cell

For high-pressure study, a diamond anvil cell (DAC, Fig. 1) was used because of its handiness and transparency from ultraviolet-visible to infrared region and also to x-ray. The applied pressure was determined by the ruby luminescence method and the peak energy of the luminescence was calculated by a polynomial fitting of the spectrum (the accuracy was  $\pm 0.1$  GPa). This DAC allow us the measurements up to 11 GPa in the temperature range between 77 and 400 K (ref. 9).

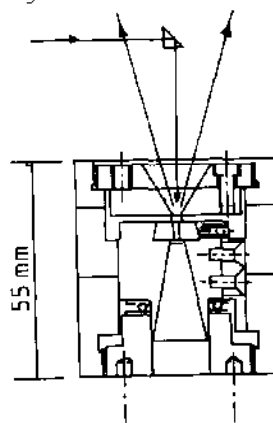


Fig.1 A diamond anvil cell (DAC, ref. 9).

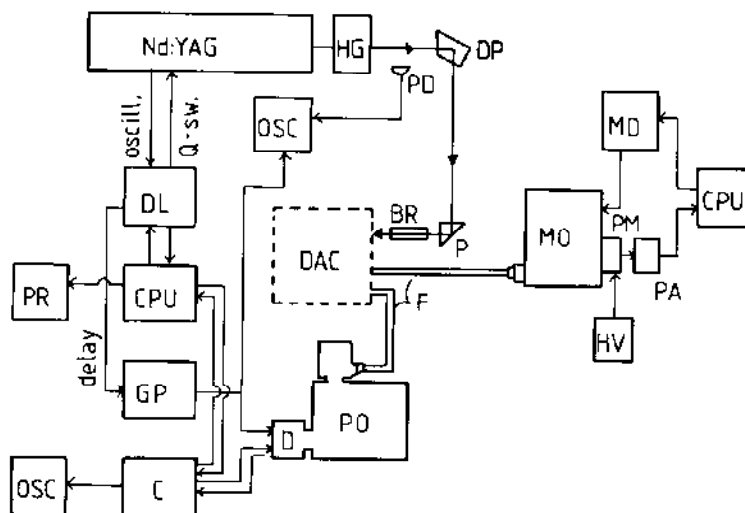


Fig.2 Block diagram of the time-resolved emission analysis system: YAG, a Nd:YAG laser (Quanta-Ray, DCR-1); HG, a harmonic generator; DP, a dispersion prism; P, a rectangular prism; BR, a beam reducer; PR, a printer or a plotter; OSC, an oscilloscope for monitoring the timing between a laser pulse and a delay or an emission decay profile (Iwatsu, TS-8123) or emission spectrum (Tektronics 475); DL, a delay generator (Stanford Research Inc., DG535); CPU, a microcomputer (Mitsubishi, Multi 16-111 or NEC, PC-9801m); D, a diode array detector (Tokyo Instruments Inc./Princeton Instruments Inc., IRY-512 spectrometric multichannel analyzer (SMA)); GP, a gate pulser (FG-110); C, a SMA controller (ST-110); PC, a polychromator (Jabin-Ybon, HR-320); F, an optical fiber; MO, a monochromator for pressure determination; PM, a photomultiplier tube (Hamamatsu, R928); HV, a high-voltage power supply; PA, a pulse amplifier and an AD converter; MD, a monochromator driver (ref. 9).

### Nanosecond time-resolved emission spectroscopy

Excitation of samples and detection of the emission from DAC were conducted by means of a backscattering configuration under a stereomicroscope or in a homemade liquid nitrogen cryostat. The emission from DAC was introduced to a polychromator through a

quartz optical fiber. Nanosecond time-resolved emission spectra were obtained by using the system which consists of a pulsed Nd:YAG laser, a gated multichannel plate/photodiode array detector (spectral multichannel analyzer, SMA) equipped with a polychromator, a controller, and a digital delay generator. The block diagram is shown in Fig.2. The time and wavelength resolution were  $\sim 5$  ns and  $\sim 0.5$  nm, respectively. A photomultiplier was used for a measurement of the emission decay profile.

Further details of the experiments have been described elsewhere (ref. 9).

### PRESSURE EFFECTS ON $\text{Pt}_2^{4-}$ CRYSTALS Pressure Dependence of Emission Spectrum of $\text{Pt}_2^{4-}$ Crystals

Emission spectra of  $\text{Pt}_2^{4-}$  crystals at various pressure are shown in Fig.3. The pressure effects on the spectral shape were reversible and reproducible upon applying and releasing pressure. With increasing pressure both the emission maxima of fluorescence ( $\nu_f$ ) and phosphorescence ( $\nu_p$ ) from  $\text{Pt}_2^{4-}$  crystals shifted almost linearly to lower energy (Fig.4). The amounts of the shifts ( $\Delta\nu/\Delta P$ ) were  $-170$  and  $-190$

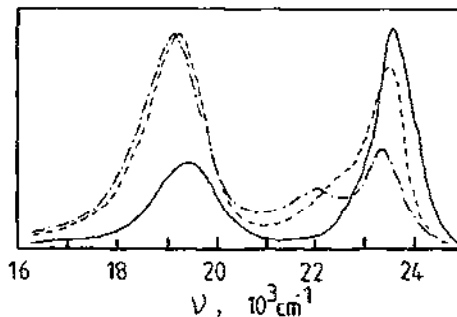


Fig.3 Emission spectra of  $\text{Pt}_2^{4-}$  crystals at atmospheric pressure (—,  $10^{-2}$  GPa), 0.8 GPa (---), and 1.5 GPa (- · -); excitation at 355 nm, gate width of SMA = 20 ns. The intensities are normalized to the highest intensity (ref. 4).

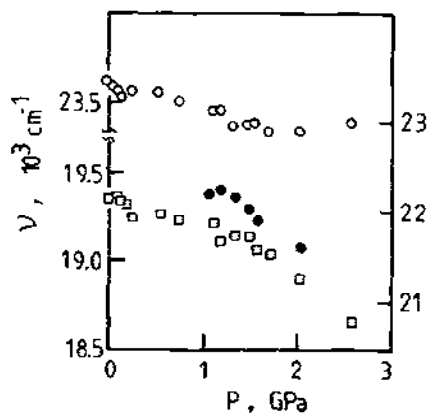


Fig.4 Emission maximum energy as a function of pressure. O: fluorescence, □: phosphorescence, and ●: new emission. Data reproduced from ref. 4.

$\text{cm}^{-1}/\text{GPa}$  for  $V_F$  and  $V_P$ , respectively. The microcrystals, which have random arrangement of  $\text{Pt}_2^{4-}$  units, showed similar pressure dependence of  $V_F$  and  $V_P$  and  $\Delta V/\Delta P$  were comparable to those for  $\text{Pt}_2^{4-}$  crystals. Therefore, these shifts in  $V_F$  and  $V_P$  are ascribed to intramolecular effect on  $\text{Pt}_2^{4-}$  structure.

For the face-to-face binuclear complex, approximate molecular orbitals can be constructed by the combination of orbitals for two square planar complexes constituting the binuclear complex (refs. 6-7, 10-11). The molecular orbital relevant to the monomeric square complex splits into two. In the case of  $\text{Pt}_2^{4-}$ , the  $d_z^2$  splits into  $d\sigma^*$  (HOMO) and  $d\sigma$ , and the  $p_z$  splits into  $p\sigma^*$  and  $p\sigma$  (LUMO). The degree of the splitting is decided by the strength on the metal-metal interaction; metal-metal distance. X-ray analysis and IR spectroscopy of  $\text{Pt}_2^{4-}$  crystals under high pressure suggest that both intra- and intermolecular Pt-Pt distances along the Pt-Pt axis are compressed (ref. 4). Thus, the applied pressure brings about the strong Pt-Pt interaction. The pressure induced lower energy shift of the emission is interpreted as the result of stronger destabilization of HOMO than that of LUMO.

The most striking feature of  $\text{Pt}_2^{4-}$  crystals is emergence of a new emission at lower energy side of the fluorescence under high pressure (Fig.3). The characteristics of this new emission were a large pressure-induced lower energy shift ( $\sim 1000 \text{ cm}^{-1}/\text{GPa}$ , Fig.4) and an immeasurably short lifetime ( $< 10$  ps). This new emission was observed only for well-grown  $\text{Pt}_2^{4-}$  crystals, but not for microcrystals or solution  $\text{Pt}_2^{4-}$  having random arrangement of  $\text{Pt}_2^{4-}$  units. In  $\text{Pt}_2^{4-}$  the electronic state of the singlet is not expected to split any more by perturbation even if spin-orbit coupling is considered. Therefore, this new emission is owing to intermolecular interaction between  $\text{Pt}_2^{4-}$  units.

In the well-grown crystals intermolecular interaction exists as observed as triplet energy migration, which is dominant under high pressure (ref. 12). The exciton in molecular crystals exists in a band close to the excitation level resulting from the condensed state of molecules. The excited state is transferred through the band and recombines with a ground state molecule at some trap site in crystals, which is observed as excimer, for example (ref. 13).  $\text{Pt}_2^{4-}$  crystals (as  $\text{K}^+$  salt) have the intermolecular Pt-Pt distance of 5.1 angstrom along the Pt-Pt axis which is roughly equivalent to the size of  $5d_z^2$  and/or  $6p_z$  atomic orbitals. While the applied pressure reduces the intermolecular distance, the interaction between  $\text{Pt}_2^{4-}$  molecules becomes stronger than at atmospheric pressure.

In the case of molecular crystals of aromatic hydrocarbons such as pyrene, it is well known that the excimer emission owing to exciton migration and subsequent trapping in excimer forming sites is observed at atmospheric

pressure. With increasing pressure, the excimer emission shifts to lower energy since the reduction of intermolecular distances increases the binding energy in the excited state and augments the repulsive potential in the Franck-Condon ground state. Excimer formation in  $\text{Pt}_2^{4-}$  crystals is unprecedented, and it is difficult to obtain direct evidence from analysis of its emission rise and decay profile. However, the finding that the new emission is observed under high pressure when the inter  $\text{Pt}_2^{4-}$  distance is comparable to or somewhat longer than the excimer forming distance in organic systems is in support of the present assignment. If  $5d_{z^2}$  and/or  $6p_z$  orbitals participate in excimer formation, excimer formation at a larger separation than in the case of organic excimers is reasonable. The new emission is characteristic of the well-grown crystals but not of the microcrystals in which the molecular arrangement is thought to be irregular. Random molecular arrangement in solid is certainly unfavorable for excimer formation. Not only for excimer formation, energy migration is suppressed in microcrystals as manifested by the absence of T-T annihilation.

#### Pressure Induced T-T Annihilation

In solution or microcrystals,  $\text{Pt}_2^{4-}$  exhibits strong phosphorescence which decays single exponentially with long lifetime ( $\sim 10$  or  $3-4 \mu\text{s}$ , respectively). In the well-grown crystals, on the other hand, the phosphorescence decay profile is non-single exponential and strongly depends on the excitation density. The lower the excitation density, the better the decay profile analysis by single exponential function. This is interpreted by T-T annihilation subsequent to triplet energy migration (ref. 14).

The energy migration process occurs via overlapped  $5d_{z^2}$  orbitals directing Pt-Pt axis in the crystals so that the efficiency (i.e., deviation of the decay profile from single exponential function) is expected to be sensitive to intermolecular  $\text{Pt}_2^{4-}$  distance. In Fig.5, the phosphorescence decay profiles of  $\text{Pt}_2^{4-}$  at several pressure are shown. With increasing pressure,

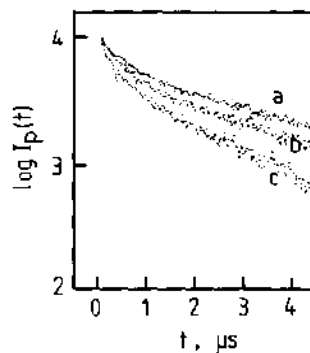


Fig.5 Phosphorescence decay profiles of  $(\text{Bu}_4\text{N})_4[\text{Pt}_2(\text{P}_2\text{O}_5\text{H}_2)_4]$  crystals at 0.03 (a), 4.41 (b) and 8.80 GPa (c).

faster and the profiles deviate from single exponential functions. As mentioned above, the applied pressure brings about changes in intermolecular Pt-Pt distance so that the rate of energy migration increases (ref. 15).

Analogous distance dependence of energy migration can be observed by varying counter cation size of  $\text{Pt}_2^{4-}$  crystals (ref. 12). Changes in the counter cations from  $\text{Na}^+$ ,  $\text{K}^+$ ,  $\text{Et}_4\text{N}^+$  to  $n\text{-Bu}_4\text{N}^+$  (increasing order of inter  $\text{Pt}_2^{4-}$  distance) result in slower phosphorescence decay and the decay profiles approach to single exponential function. The increase in the counter cation size brings about decrease in the efficiency of the energy migration.

In the case of  $\text{Pt}_2^{4-}$  crystals, application of pressure affects both inter and intramolecular Pt-Pt distance (interaction). Lower energy shifts of fluorescence and phosphorescence are due to intramolecular deformation, while the intermolecular perturbation induced the emergence of new emission band (excimer-like emission from the singlet state) as well as efficient T-T annihilation subsequent to triplet energy migration.

### PRESSURE EFFECTS ON $\text{Ru}(\text{bpy})_3^{2+}$ EMISSION IN ETHANOL-METHANOL

#### Pressure and Temperature Dependence of Emission Spectrum

At room temperature,  $\text{RuB}_3^{2+}$  shows broad and structureless emission with the maximum energy ( $\nu_{\text{em}}$ ) of  $16410 \text{ cm}^{-1}$  in ethanol-methanol (4/1, v/v). With increasing pressure,  $\nu_{\text{em}}$  shifts lower energy ( $15680 \text{ cm}^{-1}$  at 1.8 GPa, Fig.6a). The rate of lower energy shift ( $\Delta\nu_{\text{em}}/\Delta P = -390 \text{ cm}^{-1}/\text{GPa}$ ) is slightly larger than that observed in acetonitrile ( $-230 \text{ cm}^{-1}/\text{GPa}$ ) but is very much larger than the value in crystal ( $-0.2 \text{ cm}^{-1}/\text{GPa}$  below 2 GPa, ref. 16). In solution, the applied pressure induces an increase in density of the solvent and thus, in dielectric constant ( $D_s$ ), refractive index ( $n$ ), and viscosity ( $\eta$ ).  $\nu_{\text{em}}$  of  $\text{Ru}(\text{II})$  complexes is sensitive to  $D_s$  and/or  $n$ . Therefore, application of pressure to  $\text{RuB}_3^{2+}$  solution leads to stabilization of the MLCT excited state (lower energy shift of emission) through increases in  $D_s$  and/or  $n$  of the solvent (refs. 17-18). At 100 K, on the contrary, the solvent is fully rigid (glass-to-fluid transition temperature,  $T_g$ , in ethanol-methanol (4/1, v/v) is 130 K) so that the applied pressure does not influence the solvent properties appreciably. The emission spectra at 100 K are thus, almost independent of pressure as shown in Fig.6b.

In marked contrast to the results at room temperature or at 100 K, a pressure induced high energy emission shift was observed between 110 and 200 K together with sharpening of the spectrum (Fig.6c). At (0.06 GPa - 160 K), the spectrum is relatively broad with  $\nu_{\text{em}} = 16190 \text{ cm}^{-1}$  and the full width at half-maximum (fwhm) =  $3400 \text{ cm}^{-1}$  while  $\nu_{\text{em}}$  and fwhm at 0.91 GPa are 17080 and 2510

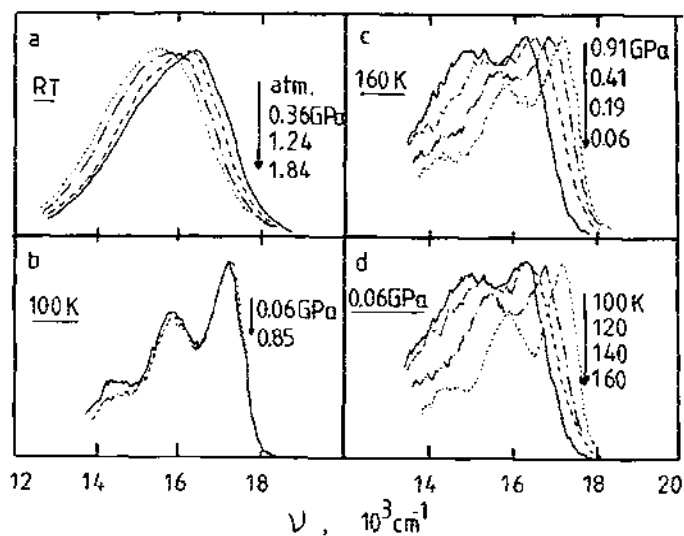


Fig.6 Emission spectra of  $\text{Ru}(\text{bpy})_3^{2+}$  in ethanol-methanol (4/1, v/v).  
Data reproduced from ref. 5.

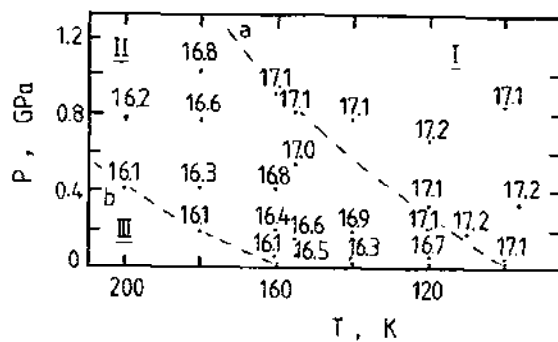


Fig.7 Pressure and temperature effects on the emission energy ( $\times 10^3 \text{ cm}^{-1}$ ) of  $\text{Ru}(\text{bpy})_3^{2+}$  in ethanol-methanol: the numbers represent emission maximum energy at a given (P-T) condition (ref. 5).



$\text{cm}^{-1}$ , respectively. At 0.91 GPa, the vibrational structures of the spectrum are well-resolved similar to the spectrum at 100 K.

Temperature dependence of the  $\text{Ru}(\text{bpy})_3^{2+}$  emission spectrum at a fixed pressure is shown in Fig.6d. At 0.06 GPa, the spectrum becomes sharper and shifts to higher energy upon cooling. The important finding is that the changes in the spectrum by cooling at a fixed pressure are quite analogous to those observed by applying pressure at a fixed temperature. Indeed, both  $\nu_{\text{em}}$  and fwhm of the spectrum at (0.06 GPa - 100 K) agree quite well with those at (0.91 GPa - 160 K). Both applying pressure and decreasing temperature bring about the similar effect on the emission spectrum; high energy shift and sharpening of the emission spectrum. The result clearly demonstrates that the emission spectral shape is determined by solvent viscosity.

$\nu_{\text{em}}$  obtained at other (P-T) conditions are summarized in Fig.7. The dashed lines, a and b in Fig.7, are contour lines corresponding to  $\nu_{\text{em}}$  to 17100 and 16100  $\text{cm}^{-1}$ , respectively. In the (P-T) region above line a, I, the emission spectrum was almost independent of P and T, giving sharp and structured emission at 17100 ~ 17200  $\text{cm}^{-1}$  similar to the spectrum at (0.06 GPa - 100 K). In the (P-T) region below line b, III, the spectrum was broad and structureless with  $\nu_{\text{em}} \sim 16100 \text{ cm}^{-1}$  regardless of P and T. In the intermediate (P-T) region, II, however,  $\nu_{\text{em}}$  and fwhm of the emission spectrum are strongly dependent on P as well as on T. At 0.06 GPa, a decrease in T from 160 to 100 K results in an increase in  $\nu_{\text{em}}$  from 16100 to 17100  $\text{cm}^{-1}$ . Similarly, at 160 K, the applied pressure gives an increase in  $\nu_{\text{em}}$  from 16100  $\text{cm}^{-1}$  at 0.06 GPa to 17100  $\text{cm}^{-1}$  at 0.91 GPa. Analogous results were obtained for other sets of (P-T). It is noteworthy that a time-dependent lower energy shift of the spectrum was observed in the (P-T) region, II.

#### Time-dependent Lower Energy Shift of Emission Maximum

Time-dependent (TD) behavior of the emission in polar solution is common phenomenon and has been currently discussed in detail on the basis of solvation dynamics around the excited solute molecules (ref. 19). Under

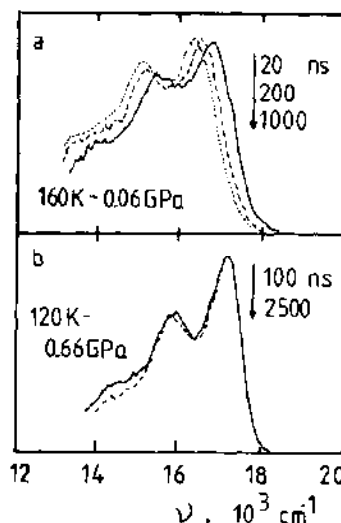


Fig.8 Time-resolved emission spectra of  $\text{Ru}(\text{bpy})_3^{2+}$  in ethanol-methanol. Data reproduced from ref. 5.

high pressure, the solvent viscosity increases with  $P$  so that the TD shift is detected at higher temperature. Fig.8 shows time-resolved emission spectra in ethanol-methanol. At (0.06 GPa - 160 K), the spectrum shifts to lower energy with increasing a delay time after excitation ( $t$ ) while the TD shift cannot be seen at (0.66 GPa - 120 K). Dependence of  $\Delta V_{\max}$  ( $V_{\text{em}}(t=0) - V_{\text{em}}(t=t')$ ) is shown in Fig.9 as well. At 0.15 GPa,  $V_{\text{em}}$  shifts to a lower energy by  $\sim 200$  or  $\sim 300 \text{ cm}^{-1}$  from  $t' = 0.1$  to  $1.1 \mu\text{s}$  at 140 or 155 K, respectively (Fig.9a). At 155 K (Fig.9b),  $\Delta V_{\max}(t' = 0.1 \sim 1.1 \mu\text{s})$  decreases with increasing  $P$  from  $\sim 200 \text{ cm}^{-1}$  at 0.07 GPa to  $\sim 50 \text{ cm}^{-1}$  at 0.54 GPa. The results manifest that determines  $\Delta V_{\max}$  and thus, the rate of solvent relaxation.

Under atmospheric pressure, the TD emission shift of  $\text{RuB}_3^{2+}$  was observed in narrow temperature region between 115 - 150 K in ethanol-methanol ( $T_g = 130 \text{ K}$ ), 120 - 170 K in 1-propanol ( $T_g = 147 \text{ K}$ ), or 160 - 230 K in 1-hexanol ( $T_g = 223 \text{ K}$ ). It is obvious that the rate of solvent relaxation is governed by  $T_g$  or  $f_p$  (freezing point) of the solvent (ref. 20). Solvent effect on the TD shift is highly consistent with  $P$  and  $T$  dependence of the emission.

Both  $P$  and  $T$  dependence of  $V_{\text{em}}$  can be satisfactorily explained by viscosity-dependent solvent relaxation. In a rigid matrix far below  $T_g$ , the motion of solvent molecules around the excited state complex is inhibited so that  $V_{\text{em}}$  is higher than that of the solvent relaxed MLCT excited state at elevated temperature. Above  $T_g$  of the medium, on the other hand, since solvent relaxation takes place within ns - ps time regime, the emission spectrum of the complex is observed at a lower energy relative to that below  $T_g$ . Large broadening of the spectrum with decreasing  $P$  or increasing  $T$  is also readily understandable as a result of time-averaging of the stabilization of the charge separated excited state with the surrounding polar solvent molecules.

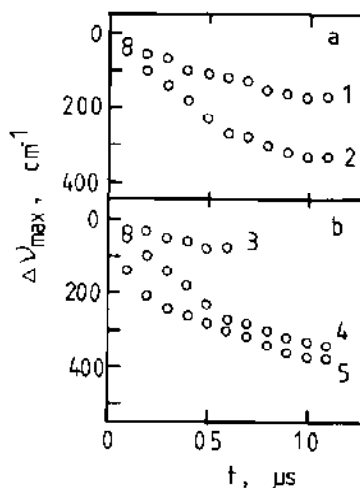


Fig.9 Temperature (a) and pressure (b) effects on time-dependent lower energy shift of  $\text{Ru}(\text{bpy})_3^{2+}$  emission in ethanol-methanol. (a) At 0.15 GPa,  $T = 140$  (1) and 155 K (2). (b) At 155 K,  $P = 0.54$  (3), 0.15 (4), and 0.07 GPa (5). Data reproduced from ref. 5.

## REFERENCES

1. Present address: Electrotechnical Laboratory, Umezono 1-1-4, Tsukuba, Ibaraki 305, Japan.
2. Present address: Microphotoconversion Project, Research Development Corporation of Japan, 15 Morimoto-cho, Shinjogamo, Sakyo-ku, Kyoto 606, Japan.
3. H.G. Drickamer, *Acc.Chem.Res.*, **19**, 329 (1986).
4. T. Hiraga, T. Uchida, N. Kitamura, H.-B. Kim, S. Tazuke, and T. Yagi, *J.Am.Chem.Soc.*, in press.
5. T. Hiraga, N. Kitamura, H.-B. Kim, S. Tazuke, and N. Mori, *J.Phys.Chem.*, **93**, 2940 (1989).
6. E.A. Roundhill, H.B. Gray, and C.-M. Che, *Acc.Chem.Res.*, **22**, 55 (1989).
7. A.P. Zipp, *Coord.Chem.Rev.*, **84**, 47 (1988).
8. A. Juris, V. Balzani, F. Barigolletti, S. Campagna, P. Bulser, and A. von Zelewsky, *Coord.Chem.Rev.*, **84**, 85 (1988).
9. T. Hiraga, T. Uchida, N. Kitamura, H.-B. Kim, T. Ikeda, and S. Tazuke, *Rev.Sci.Instrum.*, **60**, 1008 (1989).
10. K.A. Stroud, H.G. Drickamer, M.H. Zietlow, H.B. Gray, and B.I. Swanson, *J.Am.Chem.Soc.*, **111**, 56 (1989).
11. M. Fetterolf, A.E. Friedman, Y.-Y. Yang, H. Offer, and P.C. Ford, *J.Phys.Chem.*, **92**, 3760 (1988).
12. T. Uchida, H.-B. Kim, T. Hiraga, and S. Tazuke, *J.Am.Chem.Soc.*, in press.
13. J.E. Birks and A.A. Kazzaz, *Proc.Roy.Soc.*, **A304**, 291 (1968).
14. Y. Tanaka and T. Azumi, *Inorg.Chem.*, **25**, 248 (1986); *Chem.Phys.Lett.*, **132**, 357 (1985).
15. T. Uchida, H.-B. Kim, and S. Tazuke, in preparation.
16. H. Yersin and E. Gallhuber, *Inorg.Chem.*, **23**, 3475 (1984).
17. E.M. Kober, B.P. Sullivan, and T.J. Meyer, *Inorg.Chem.*, **23**, 2098 (1984).
18. N. Kitamura, M. Sato, H. B. Kim, R. Ohts, and S. Tazuke, *Inorg.Chem.*, **27**, 651 (1988).
19. J.D. Simon, *Acc.Chem.Res.*, **21**, 128 (1988).
20. H.-B. Kim, N. Kitamura, and S. Tazuke, *J.Phys.Chem.*, in press.